

Laser-assisted ion-atom collisions: Plateau, cutoff, and multiphoton peaks

Marcelo F. Ciappina

Max Planck Institute for the Physics of Complex Systems, Nöthnitzer Strasse 38, D-01187 Dresden, Germany

Lars Bojer Madsen

Lundbeck Foundation Theoretical Center for Quantum System Research, Department of Physics and Astronomy, University of Aarhus, 8000 Aarhus C, Denmark

(Received 21 March 2007; revised manuscript received 24 October 2007; published 13 February 2008; corrected 25 February 2008)

We study ionization in laser-assisted high-energy nonrelativistic ion-atom collisions and show that the low-energy angular differential electron spectrum may be enhanced by five orders of magnitude by an external field of strength less than 1/100 of the atomic field. With increasing strength of the assisting field, the energy spectrum develops a plateau with a characteristic cutoff. In the plateau region we predict distinct multiphoton peaks separated by the photon energy of the assisting field. In the present laser-assisted continuum-distorted-wave eikonal-initial-state theory, this effect may be related to the dynamics in the two-body electron-projectile subsystem. The laser-assisted distorted wave Born and first Born approximation do not account for the phase-distortion of the target electron by the incoming projectile and consequently the associated plateau, cutoff, and multiphoton features are not predicted by these latter theories.

DOI: [10.1103/PhysRevA.77.023412](https://doi.org/10.1103/PhysRevA.77.023412)

PACS number(s): 34.80.Qb, 34.50.Rk

I. INTRODUCTION

When a high-energy ion collides with an atomic target, sufficient energy may be picked up to ionize the atom. The study of such processes is a matured field with detailed understanding of the dynamics of the particles involved [1]. A related field of research is strong-field physics where an atom may break and emit an electron when subject to an intense laser field. In the continuum, the electron propagates mainly subject to the external field, which may steer it back to the parent ion [2]. Upon recollision, the electron may recombine and stimulate the emission of coherent high-energy radiation through the process of high-harmonic generation, it may, if energetic enough, induce multiple ionization, or it may absorb additional photons. In the latter case the result is a characteristic above threshold ionization (ATI) spectrum with an extended plateau region and a cutoff at about 10 times the quiver energy of the free electron in the field, U_p .

In the present work, we study the electron spectrum generated in high-energy ionizing laser-assisted ion-atom collisions. We report on the emergence of a plateau, a cutoff in the energy spectrum, and more surprisingly characteristic multiphoton peaks separated by the photon energy of the assisting field. In this sense we rediscover some of the features well-known from strong-field ATI spectra. The physics, however, turns out to be very different. In fact our assisting field is weak, at maximum about 1/100 the strength of a typical atomic field, and yet so many photons are exchanged that the low energy part of the angular differential electron spectrum may be affected dramatically: in certain cases enhanced by up to five orders of magnitude. The reason for the strong coupling to the external field is basically due to the low frequency of the assisting CO₂ laser, $\hbar\omega=0.117$ eV. The field-free cross section is a continuous, and on the scale of ω , smooth function of the final kinetic energy of the electron and therefore the emergence of a comb of multiphoton peaks is *a priori* counterintuitive. As we shall see, however, the strong free-free coupling leads to considerable modification

of the electron dynamics in the two-body electron-projectile subsystem and this modification is the effect that courses the plateau, cutoff, and the quantized multiphoton peaks in the spectrum.

We are not alone in the study of laser-assisted processes. For example, in high-harmonic generation from laser-assisted ion-atom collisions extended plateau and additional cutoffs in the harmonic signal were reported [3]. The problem of laser-assisted ion-atom collisions was examined theoretically (see, e.g., [4–12] and references therein) but not in the present regime and not with the dramatic enhancement effects reported here. Classical and one-dimensional (1D) quantum simulations have shown that it is possible to redistribute the energy among the collision partners and that the projectile can gain energy in the process [13]; we find similar behavior in our quantum theory.

This paper is organized as follows. In the next section we describe the laser-assisted continuum-distorted-wave, eikonal-initial state (LA-CDW-EIS) theory. We include a discussion of how the laser-assisted distorted-wave Born (LA-DWB) and first Born (LA-FBA) approximations are obtained from the LA-CDW-EIS as the limiting case. In Sec. III we discuss the LA-CDW-EIS results and we compare them with the predictions of the LA-DWB and LA-FBA approaches. Section IV concludes.

II. LASER-ASSISTED CONTINUUM-DISTORTED-WAVE, EIKONAL-INITIAL-STATE (LA-CDW-EIS) THEORY

We restrict the study to the case of H(1s) targets and structureless ion projectiles. The assisting CO₂ laser field is described as a continuous wave with vector potential

$$\mathbf{A}(t) = \boldsymbol{\epsilon} A_0 \cos(\omega t), \quad (1)$$

where $\boldsymbol{\epsilon}$ is the linear polarization, A_0 the amplitude, and ω the angular frequency of the field (atomic units $\hbar=|e|=m_e=a_0=1$ are used unless stated otherwise). The electric field is

obtained as $\mathbf{F}(t) = -\partial_t \mathbf{A}(t)$ and, consequently, $F_0 = A_0 \omega$. The laser field strengths considered are low compared with the Coulomb interaction between the collision partners. Hence the field-dressing of the initial atomic state can be neglected, no direct laser-induced ionization occurs, and it is uniquely the incoming projectile that triggers the ionization process. The projectile is so heavy that its motion is not directly influenced by the external field; the laser field is only important in the description of the final state of the continuum electron. This outgoing electron evolves in the laser field and in the Coulomb fields of the parent ion and the projectile. We describe the collision part of the process with a laser-modified version of the continuum distorted wave-eikonal initial state (CDW-EIS) theory. In the field-free case this theory models accurately the whole energy spectrum and takes into some consideration both the electron-projectile and electron-target Coulomb interactions [14]. Despite the successes of the CDW-EIS theory to field-free ion-atom collision processes [1, 14–16], it has not before been applied to the problem of laser-assisted collisions.

In the following we introduce the approximations used in our model. We use Jacobi coordinates (see, e.g., [16]) with the position of the electron with respect to the target (projectile) denoted by \mathbf{r}_T (\mathbf{r}_p). Further, the position of the projectile (target) with respect to the center of mass of the initial (final) subsystem is denoted by \mathbf{R}_T (\mathbf{R}_p). In collisions with heavy projectiles this choice of coordinates is convenient since it allows one to separate the electronic and the incoming projectile motions (see discussion below).

The S -matrix amplitude in the LA-CDW-EIS model is given by

$$S_{if}^{LA-CDW-EIS} = -i \int_{-\infty}^{+\infty} dt \langle \Psi_f^{LA-CDW,(-)} | W_i | \Psi_i^{EIS,(+)} \rangle, \quad (2)$$

where $\Psi_i^{EIS,(+)}$ and $\Psi_f^{LA-CDW,(+)}$ are the initial and final states of the collision system, which account for the presence of the laser field in the sense discussed below and fulfill the usual asymptotic limit for the field-free collision system, i.e., outgoing (incoming) boundary conditions for the initial (final) state. W_i is the perturbation of the field-free CDW-EIS formalism in its *prior* form (see the discussion below). To proceed explicitly with the S -matrix calculations, i.e., Eq. (2), we note that in collisions with heavy particles $\mathbf{R}_T \approx \mathbf{R}_p = \mathbf{r}_T - \mathbf{r}_p$ to order $1/M_{T,p}$ [16]. This allows us to change the integration in Eq. (2) over \mathbf{R}_T to an integration over \mathbf{r}_p , resulting in generalized Nordsieck-type 3D integrals for both \mathbf{r}_T and \mathbf{r}_p (see the Appendix).

The total initial state in Eq. (2) is written as

$$\Psi_i^{EIS,(+)}(\mathbf{r}_T, \mathbf{r}_p, t) = \Phi_{\mathbf{K}_i}(\mathbf{R}_T, t) \psi_{i,\mathbf{v}}^{EIS,(+)}(\mathbf{r}_T, \mathbf{r}_p, t), \quad (3)$$

where

$$\Phi_{\mathbf{K}_i}(\mathbf{R}_T, t) = (2\pi)^{-3/2} \exp(i\mathbf{K}_i \cdot \mathbf{R}_T) \exp(-iE_i t) \quad (4)$$

is a plane wave representing the incoming projectile with $E_i = K_i^2 / (2\mu_i)$ and $\mu_i = M_p(M_T + 1) / (M_p + M_T + 1)$, M_p (M_T) being the mass of the projectile (target) and $\psi_{i,\mathbf{v}}^{EIS,(+)}(\mathbf{r}_T, \mathbf{r}_p, t)$ the initial electronic state. In this state, the

asymptotic form of the Coulomb distortion, the so-called eikonal phase, is used to describe the electron-projectile interaction. Consequently,

$$\psi_{i,\mathbf{v}}^{EIS,(+)}(\mathbf{r}_T, \mathbf{r}_p, t) = \mathcal{E}_{\mathbf{v}}^{(+)}(\mathbf{r}_p) \phi_i(r_T) \exp(-i\epsilon_i t), \quad (5)$$

where

$$\mathcal{E}_{\mathbf{v}}^{(+)}(\mathbf{r}_p) = \exp\left(-i \frac{Z_p}{v} \ln(vr_p - \mathbf{v} \cdot \mathbf{r}_p)\right) \quad (6)$$

is the eikonal phase, satisfying outgoing wave boundary conditions, \mathbf{v} being the velocity of the incoming projectile and Z_p its charge. Further, $\phi_i(r_T)$ represents the initial $1s$ state of the hydrogen target with energy $\epsilon_i = -1/2$ a.u. The laser parameters are chosen in a such a way that they do not affect the atomic ground state and we neglect such *dressing* effect accordingly.

The full final state is cast into the form

$$\Psi_f^{LA-CDW,(-)}(\mathbf{r}_T, \mathbf{r}_p, t) = \Phi_{\mathbf{K}_f}(\mathbf{R}_p, t) \psi_{f,\mathbf{k}}^{CDW,(-)}(\mathbf{r}_T, \mathbf{r}_p, t). \quad (7)$$

In Eq. (7), the projectile is described by a plane wave with momentum \mathbf{K}_f and energy $E_f = K_f^2 / (2\mu_f)$, where $\mu_f = M_T(M_p + 1) / (M_p + M_T + 1)$:

$$\Phi_{\mathbf{K}_f}(\mathbf{R}_p, t) = (2\pi)^{-3/2} \exp(i\mathbf{K}_f \cdot \mathbf{R}_p) \exp(-iE_f t), \quad (8)$$

and $\psi_{f,\mathbf{k}}^{CDW,(-)}(\mathbf{r}_T, \mathbf{r}_p, t)$ is the electronic wave function for the final state that also accounts for the presence of the laser. The interaction of the continuum final-state electron with the electromagnetic field is described in the length gauge and dipole approximation

$$H_I = \mathbf{r}_T \cdot \mathbf{F}(t). \quad (9)$$

The electronic wave function $\psi_{f,\mathbf{k}}^{CDW,(-)}(\mathbf{r}_T, \mathbf{r}_p, t)$ is cast into the form

$$\psi_{f,\mathbf{k}}^{CDW,(-)}(\mathbf{r}_T, \mathbf{r}_p, t) = \psi_{\mathbf{k}}^{2C,(-)}(\mathbf{r}_T, \mathbf{r}_p) \mathcal{L}_{\mathbf{v}}(\mathbf{r}_T, t) \exp(-i\epsilon_f t), \quad (10)$$

$\epsilon_f = k^2/2$ being the asymptotic energy of the outgoing electron and $\psi_{\mathbf{k}}^{2C,(-)}(\mathbf{r}_T, \mathbf{r}_p)$ a *two center* Coulomb wave function satisfying incoming boundary conditions [15], i.e.,

$$\psi_{\mathbf{k}}^{2C,(-)}(\mathbf{r}_T, \mathbf{r}_p) = \Phi_{\mathbf{k}}(\mathbf{r}_T) \mathcal{L}_T^-(\mathbf{r}_T, \mathbf{k}) \mathcal{L}_p^-(\mathbf{r}_p, \mathbf{k}_p), \quad (11)$$

with

$$\Phi_{\mathbf{k}}(\mathbf{r}_T) = (2\pi)^{-3/2} \exp(i\mathbf{k} \cdot \mathbf{r}_T) \quad (12)$$

a plane wave,

$$\mathcal{L}_C^-(\mathbf{r}_T, \mathbf{k}) = N(\alpha_T) {}_1F_1(-i\alpha_T, 1, -ikr_T - i\mathbf{k} \cdot \mathbf{r}_T) \quad (13)$$

the Coulomb distortion of the electron by the target, $\alpha_T = Z/k$, $N(\alpha_T) = \exp(\pi\alpha_T/2) \Gamma(1-i\alpha_T)$ the Coulomb normalization factor for the electron-target interaction, Z the charge of the residual ionized atom, and the ${}_1F_1$ the Kummer function [17]. Furthermore,

$$\mathcal{L}_p^-(\mathbf{r}_p, \mathbf{k}_p) = N(\alpha_p) {}_1F_1(-i\alpha_p, 1, -ik_p r_p - i\mathbf{k}_p \cdot \mathbf{r}_p), \quad (14)$$

with $\mathbf{k}_p = \mathbf{k} - \mathbf{v}$ the momentum of the electron with respect to the projectile and $N(\alpha_p)$ the Coulomb normalization factor for the electron-projectile interaction, describes the Coulomb distortion for the electron-projectile pair.

Finally in Eq. (10),

$$\mathcal{L}_v(\mathbf{r}_T, t) = \exp\left(i\mathbf{A} \cdot \mathbf{r}_T - i\mathbf{k} \cdot \int^t \mathbf{A}(t') dt' - \frac{i}{2} \int^t A^2(t') dt'\right) \quad (15)$$

is the Volkov phase stemming from the interaction of the electron with the electromagnetic field. The Volkov phase in Eq. (15) corresponds to the situation where the interaction with the electromagnetic field is formulated in the length gauge, i.e., as in Eq. (9). Using an appropriate unitary transformation it is possible to show that the theory formulated in this way is gauge invariant [4]. We see that $\mathcal{L}_v(\mathbf{r}_T, t) = 1$ in the case of the vanishing field. If the phase factor in Eq. (15) is multiplied by a plane wave state, one obtains the Volkov state of a free-electron in a laser field. In the case we consider here, the Coulomb potentials corresponding to the electron-target and the electron-projectile are important and no exact solution is available for an electron in combined Coulomb and laser fields. The Coulomb-Volkov ansatz has been considered within the strong-field approximation [18,19] (see also Ref. [20] for a recent reference).

The perturbation W_i in the CDW-EIS formalism can be obtained doing the separation of the field-free Hamiltonian H_i in the form

$$H_i = H_i^0 + U_i + W_i, \quad (16)$$

where we have introduced a *distortion* potential U_i in such a way that

$$\left(H_i^d - i\frac{\partial}{\partial t}\right)\psi_{i,v}^{EIS,(+)} = 0, \quad (17)$$

with $H_i^d = H_i^0 + U_i$. A similar treatment can be done for the final state $\psi_{f,k}^{CDW,-}$, but we do not reproduce it here since we are interested only in the prior version of the CDW-EIS approach (see, e.g., [15]). The remaining perturbation W_i can be written now as [16]

$$W_i = -\frac{1}{2}\nabla_{\mathbf{r}_p}^2 - \nabla_{\mathbf{r}_T} \cdot \nabla_{\mathbf{r}_p}. \quad (18)$$

The next step to proceed is to write the Volkov phase of Eq. (15) by expressing it through a Fourier series expansion. This is done by using the generating function of the integer Bessel function [17,21]. Consequently we can write Eq. (15) as

$$\exp\left(i\frac{\mathbf{F}_0 \cdot \mathbf{k}}{\omega^2} \sin(\omega t)\right) = \sum_{n=-\infty}^{+\infty} J_n(\alpha_0 \cdot \mathbf{k}) \exp(in\omega t), \quad (19)$$

$$\exp\left(\frac{i}{2} \int dt' A^2(t')\right) = \exp\left(i\frac{F_0^2}{4\omega^2} t\right) \sum_{l=-\infty}^{+\infty} J_l\left(\frac{U_p}{2\omega}\right) \exp(2il\omega t) \quad (20)$$

and

$$\exp[-i\mathbf{A}_0 \cdot \mathbf{r}_T \cos(\omega t)] = \sum_{m=-\infty}^{+\infty} J_m(-\mathbf{A}_0 \cdot \mathbf{r}_T) \times \exp[im(\omega t + \pi/2)], \quad (21)$$

where we have defined $\alpha_0 = \mathbf{A}_0/\omega$ as the quiver radius and $U_p = F_0^2/4\omega^2$ is the ponderomotive energy. In Eqs. (19)–(21) $J_i(x)$, ($i=n, l, m$) are Bessel functions of integer order i . Collecting the expressions (19)–(21) the field-dependent phase (15) results in

$$\mathcal{L}_v(\mathbf{r}_T, t) = \exp(iU_p t) \sum_{n,l,m=-\infty}^{\infty} J_n(\alpha) J_l[-\beta(\mathbf{r}_T)] J_m(\delta) \times \exp[in\omega t + il(\omega t + \pi/2) + 2im\omega t], \quad (22)$$

where $\alpha = |\alpha_0 \cdot \mathbf{k}|$, $\beta(\mathbf{r}_T) = \mathbf{A}_0 \cdot \mathbf{r}_T$, and $\delta = U_p/2\omega$. The triple sum in Eq. (22) can be reduced to a double one using the Graf theorem for the Bessel functions (see, e.g., [5]),

$$\mathcal{L}_v(\mathbf{r}_T, t) = \exp(iU_p t) \sum_{n,m=-\infty}^{\infty} J_n[-w(\mathbf{r}_T)] J_m(\delta) \quad (23)$$

$$\times \exp\{in[\omega t - \chi(\mathbf{r}_T)] + 2im\omega t\} \quad (24)$$

where

$$w(\mathbf{r}_T) = \sqrt{\alpha + \beta(\mathbf{r}_T)}, \quad (25)$$

$$\tan \chi(\mathbf{r}_T) = \frac{\beta(\mathbf{r}_T)}{\alpha}. \quad (26)$$

In directions where the wave vector \mathbf{k} and the quiver radius α_0 are nonorthogonal, however, we have for energies larger than ≈ 30 eV, $\mathbf{k} \cdot \alpha_0 \gg \mathbf{A}_0 \cdot \mathbf{r}_T$. This allows us to reduce $w(\mathbf{r}_T) \approx \alpha$ and $\tan \chi(\mathbf{r}_T) \approx \chi(\mathbf{r}_T) = \frac{\beta(\mathbf{r}_T)}{\alpha}$.

The resulting S -matrix in the LA-CDW-EIS formalism reads

$$S_{if}^{LA-CDW-EIS} = -2\pi i T_{if(n,m)}^{LA-CDW-EIS}(\mathbf{k}, \mathbf{q}_n) \quad (27)$$

$$\times \delta[E_i - E_f + \epsilon_f - \epsilon_i + (n+2m)\omega + U_p], \quad (28)$$

where $T_{if(n,m)}^{LA-CDW-EIS}(\mathbf{k}, \mathbf{q}_n)$ reads

$$T_{if(n,m)}^{LA-CDW-EIS}(\mathbf{k}, \mathbf{q}_n) = \sum_{n,m=-\infty}^{\infty} J_n(\alpha) J_m(\delta) \mathcal{T}_{n,m}^{CDW-EIS}(\mathbf{k}, \mathbf{q}_n), \quad (29)$$

$\mathcal{T}_{n,m}^{CDW-EIS}(\mathbf{k}, \mathbf{q}_n)$ being the field-free CDW-EIS T matrix but now evaluated at the *generalized* momentum transfer [10]

$$\mathbf{q}_n = \mathbf{q} + n\Delta, \quad (30)$$

that in addition to \mathbf{q} , includes a laser-induced shift

$$\Delta = \omega \boldsymbol{\epsilon} / \mathbf{k} \cdot \boldsymbol{\epsilon}. \quad (31)$$

In virtue of the form of the perturbation potential W_i , Eq. (18), it is possible to write $\mathcal{T}_{n,m}^{CDW-EIS}(\mathbf{k}, \mathbf{q}_n)$ as

$$\mathcal{T}_{n,m}^{CDW-EIS}(\mathbf{k}, \mathbf{q}_n) = I^{CDW-EIS}(\mathbf{q}_n) + J^{CDW-EIS}(\mathbf{q}_n), \quad (32)$$

where

$$I^{CDW-EIS}(\mathbf{q}_n) = I_P^{CDW-EIS}(\mathbf{q}) I_T^{CDW-EIS}(\mathbf{q}_n) \quad (33)$$

is a combination of *scalar* integrals $I_P^{CDW-EIS}(\mathbf{q})$ and $I_T^{CDW-EIS}(\mathbf{q}_n)$ and

$$J^{CDW-EIS}(\mathbf{q}_n) = \mathbf{J}_P^{CDW-EIS}(\mathbf{q}) \cdot \mathbf{J}_T^{CDW-EIS}(\mathbf{q}_n) \quad (34)$$

is a scalar product of *vectorial* integrals $\mathbf{J}_P^{CDW-EIS}(\mathbf{q})$ and $\mathbf{J}_T^{CDW-EIS}(\mathbf{q}_n)$. As can be seen in Eqs. (33) and (34) in the CDW-EIS formalism it is possible to separate the contributions of the different subsystems, in our case electron-projectile and electron-target. This splitting will be important in the sense that it allows us to understand the differences between the theoretical schemes we are using to model our laser-assisted process (see next section). Explicit expressions for $I_P^{CDW-EIS}(\mathbf{q})$ and $I_T^{CDW-EIS}(\mathbf{q}_n)$ as well as for $\mathbf{J}_P^{CDW-EIS}(\mathbf{q})$ and $\mathbf{J}_T^{CDW-EIS}(\mathbf{q}_n)$ are given in the Appendix. Finally note that, although \mathbf{q}_n does not depend directly on the m index, the z component of \mathbf{q} is m -dependent via $q_z = [\epsilon_f - \epsilon_i + (n + 2m)\omega + U_p]/v$ (see details below), and consequently $\mathcal{T}_{n,m}^{CDW-EIS}(\mathbf{k}, \mathbf{q}_n)$ will have an n and m dependence.

To proceed, we construct the cross section corresponding to the differential electron spectrum. With the present $(2\pi)^{-3/2}$ normalization of the continuum states, we obtain [22]

$$\frac{d\sigma^{(LA-CDW-EIS)}}{d\mathbf{k}} = \frac{(2\pi)^4}{v} \sum_{n,m=-\infty}^{\infty} \int d\boldsymbol{\eta} |\tilde{J}_{n,m} \mathcal{T}_{if(m,n)}^{LA-CDW-EIS}(\mathbf{k}, \mathbf{q}_n)|^2, \quad (35)$$

where $\tilde{J}_{n,m} = J_n(\alpha) J_m(\delta)$ and we have utilized the energy conserving δ function to reduce the dimension of the integral by writing $\mathbf{q} = \boldsymbol{\eta} + q_z \hat{z}$, where $\boldsymbol{\eta}$ is perpendicular to the projectile velocity \mathbf{v} ($\boldsymbol{\eta} \cdot \mathbf{v} = 0$) and q_z is the parallel component of \mathbf{q} . Since $E_i - E_f \approx \mathbf{v} \cdot \mathbf{q}$ for high-energy ion-atom collisions, it follows that

$$\begin{aligned} \delta[E_i - E_f + \epsilon_f - \epsilon_i + (n + 2m)\omega + U_p] \\ = \frac{1}{v} \delta[q_z - (\epsilon_f - \epsilon_i + (n + 2m)\omega + U_p)/v], \end{aligned} \quad (36)$$

and hence

$$q_z = [\epsilon_f - \epsilon_i + (n + 2m)\omega + U_p]/v. \quad (37)$$

A few remarks on the result in Eq. (35) are in order. First of all, we note that the summations run from minus infinity to plus infinity. The positive summation indices correspond to photon absorption, i.e., in the interaction of the continuum electron with the field, the electron increases its energy. The negative summation indices correspond to the opposite situation where the electron-field interaction in the vicinity of the atomic potential leads to a net stimulated emission of

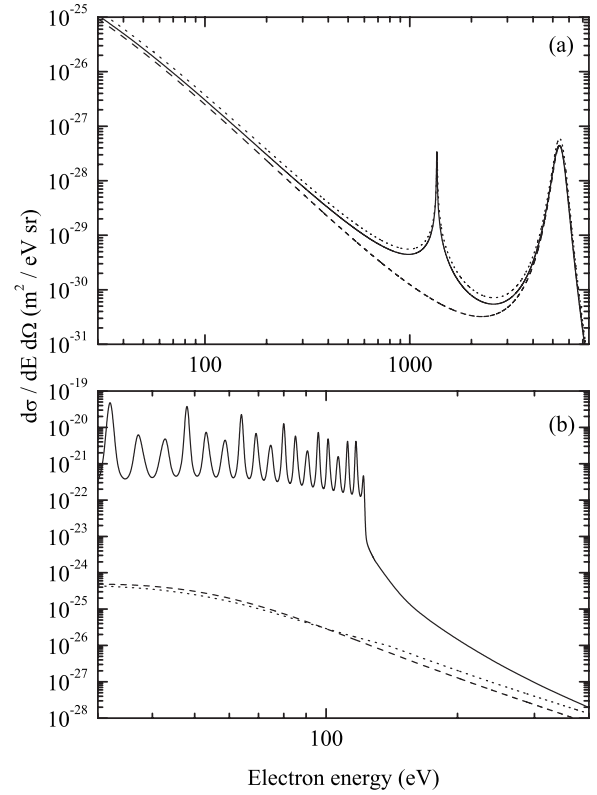


FIG. 1. Electron emission spectrum in the laser-assisted ion-atom collision $p^+ + \text{H}(1s) \rightarrow p^+ + p^+ + e^-$. The velocity of the projectile is $v = 10$ a.u. and the electron emission angle is $\theta_k = 0^\circ$. In (a) we show the field-free case. Full curve: CDW-EIS, dotted curve: DWB, and broken curve: FBA. In (b) we show the laser-assisted angular differential cross sections. The laser is a CO_2 laser ($\omega = 0.0043$ a.u.), linearly polarized in the direction of the incoming projectile velocity, i.e., $\theta_f = 0^\circ$ and has a field strength $F_0 = 0.008$ a.u. Full curve: LA-CDW-EIS, dotted curve: LA-DWB, and broken curve: LA-FBA.

photons. This phenomena was observed experimentally many years ago in laser-assisted electron-atom scattering where multiphoton emission and absorption of up to about ten photons was measured in the electron spectrum [23]. The infinity of the limits, formally introduced by the Fourier-Bessel expansion in Eqs. (19)–(21), does not pose a problem in practice, since the final magnitude of the argument of the Bessel function terminates the summation a few integers above the absolute value of the Bessel function argument.

We also note that in the limit of vanishing external field, the vector potential A_0 , the quiver radius α_0 , and the momentum transfer shift $n\Delta$ all tend to zero. Since $J_n(0) = \delta_{n,0}$, it then follows that the cross section in the laser-assisted CDW-EIS model reduces to the field-free cross section. One more remark is that, although Eq. (29) presents a product in Bessel functions and a field-free T matrix evaluated at a laser-shifted momentum, the latter is not independent of the laser field and consequently no simple sum-rule based on $\sum_l J_l(x)^2 = 1$ exists [24]. Accordingly no adding up of the laser-assisted cross sections to the field-free one is expected nor predicted [see Fig. 1 and Eq. (39) below].

A. Laser-assisted distorted wave Born (LA-DWB) and first Born approximation (LA-FBA)

We conclude this section with a brief summary of how to obtain the LA-DWB and LA-FBA from the LA-CDW-EIS theory. For a detailed discussion of the LA-DWB and LA-FBA approaches we refer the reader to Ref. [10] and references therein.

The LA-DWB formulation is obtained from the LA-CDW-EIS by neglecting the Coulomb interaction between the target electron and the projectile in the initial state, i.e., by replacing the eikonal phase in Eq. (5) by unity. On the other hand, the LA-FBA is obtained from the LA-CDW-EIS by neglecting the eikonal phase as above and the Coulomb distortion factor \mathcal{L}_p^- of Eq. (11) in the definition of the final state of the outgoing electron. We note that it is possible to calculate the integrals in the LA-DWB and LA-FBA formalisms doing the replacement stated above in the expressions written in the Appendix. In both formulations, i.e., in the LA-DWB and the LA-FBA, the Coulomb interaction between the target electron and the projectile is considered as a perturbation in the initial channel. What will turn out to be important for the present discussion is that neither the LA-DWB nor the LA-FBA account for the interaction between the target electron and the projectile in the initial state.

III. RESULTS AND DISCUSSION

We start the results section showing the predictions of the different approximations in the field-free and laser assisted cases. In Fig. 1(a), we show a typical electron emission spectrum for the field-free collision $p^+ + H(1s) \rightarrow p^+ + p^+ + e^-$. The electron emission angle is $\theta_k = 0^\circ$ and the projectile velocity is $v = 10$ a.u. It is well-known that the simpler first-order theories like the first Born approximation (FBA) and the distorted wave Born (DWB) converge toward the CDW-EIS theory for high continuum electron velocity in the final state in the field-free case (see, e.g., Refs. [1,15] and references therein). This convergence is clearly seen in Fig. 1(a). The laser-modifications of the electron capture to the continuum (ECC) at (~ 1360 eV) and the binary encounter (BE) at (~ 5440 eV) peaks were discussed elsewhere [4,5,10]. In Fig. 1(b) we concentrate on the differences in LA-CDW-EIS, LA-DWB, and LA-FBA in the low energy part of the electron spectrum. The laser is a CO₂-type laser ($\omega = 0.0043$ a.u.) and is linearly polarized in the direction of the incoming projectile velocity, i.e., $\theta_F = 0^\circ$. We show in Fig. 1(b) the laser-assisted cross section for the $F = 0.008$ a.u. situation in the LA-CDW-EIS, LA-DWB, and LA-FBA theories. We see, as expected, how the theories converge for energy above the cutoff (see the discussion below). Only the LA-CDW-EIS theory captures the cutoff and plateau features. This is because the other theories do not account for the Coulomb interaction in the initial e - P channel. In agreement with earlier work [8], we find that the low-energy part of the spectrum is only modestly modified in the LA-FBA and LA-DWB theories. This marked difference in the predictions of the different theories highlights that an experimental investigation of the processes considered here would provide a very delicate test of theory.

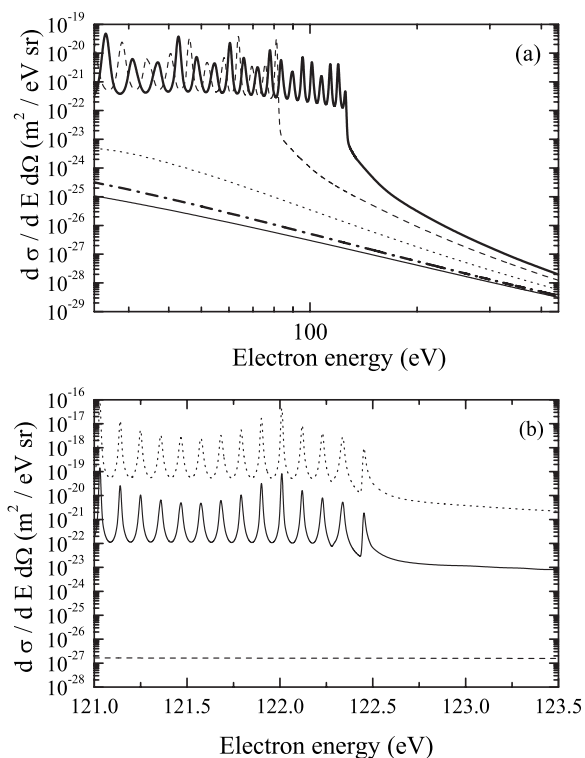


FIG. 2. Angular differential electron emission spectrum in laser-assisted $p^+ + H(1s) \rightarrow p^+ + p^+ + e^-$ collisions calculated with the LA-CDW-EIS theory. The projectile and electron parameters are the same as in Fig. 1. (a) Cross sections for increasing field strength. Lower full curve: field-free, dashed-dotted curve: $F_0 = 0.002$ a.u. (1.4×10^{11} W/cm²), dotted curve: $F_0 = 0.005$ a.u. (8.78×10^{11} W/cm²), dashed curve: $F_0 = 0.007$ a.u. (1.72×10^{12} W/cm²), and upper full curve: $F_0 = 0.008$ a.u. (2.25×10^{12} W/cm²). For increasing field strength we see a strong enhancement of the cross section and the formation of a plateau with a characteristic cutoff (see text). (b) Cutoff region on an expanded energy scale for $F_0 = 0.008$ a.u.. The energy difference between the peaks is the photon energy. Full curve: full LA-CDW-EIS T matrix, dotted curve: electron-projectile component of the LA-CDW-EIS T matrix, and dashed curve: electron-target component of the LA-CDW-EIS T matrix (see text).

We specialize our analysis on the low energy region of the spectrum, i.e., on electron energies below the ECC. Furthermore, we only investigate the predictions of the LA-CDW-EIS theory developed in Sec. II. In Fig. 2 we show the angular differential electron spectrum resulting from proton impact on H(1s) without and with the assisting CO₂ laser field. The projectile velocity is the same as in Fig. 1. In Fig. 2(a) we see how the low-energy part of the angular differential cross section is enhanced dramatically as the field strength increases. In particular for the highest field strengths we observe a plateau extending from the lowest energies considered and to a cutoff energy above which the angular differential cross section is less dramatically enhanced. The modulations at the ~ 5 eV scale in the plateau in Fig. 2(a) are due to the final energy resolution used in our calculations (see the discussion below).

In a zoomed graph, Fig. 2(b), we show how the spectrum below the cutoff is characterized by peaks separated by ex-

actly a single photon energy (minor deviations to 0.117 eV are due to the final energy resolution).

Besides the full curve in Fig. 2(b), which shows the result of the full LA-CDW-EIS T -matrix element, we use that the LA-CDW-EIS T matrix can be analyzed in a product of factors corresponding to the two-body electron-target (dashed curve), i.e., $I_T^{CDW-EIS}(\mathbf{q})$ and $\mathbf{J}_T^{CDW-EIS}(\mathbf{q})$, and electron-projectile (dotted curve), i.e., $I_P^{CDW-EIS}(\mathbf{q})$ and $\mathbf{J}_P^{CDW-EIS}(\mathbf{q})$, subsystems [14–16], and show the cross section resulting from the T -matrix factors associated with these individual subsystems.

By comparison between the dotted, dashed, and full curves in Fig. 2(b) we conclude that the plateau, cutoff, and multiphoton peaks result from the electron-projectile terms. Performing a more detailed analysis using the formulas of the Appendix it is possible to factorize the contribution of the initial and final electron-projectile part from the $I_P^{CDW-EIS}(\mathbf{q})$ and $\mathbf{J}_P^{CDW-EIS}(\mathbf{q})$. Based in the results shown in Fig. 1, where we have compared the predictions of the LA-CDW-EIS, LA-DWB, and LA-FBA, we can deduce that the exact origin of the laser-induced effects is the electron-projectile interaction in the initial state, since for the final electron-projectile subsystems the three models employed have the same electronic states (see the discussion of Sec. II A).

We now set out to explain the effects in Fig. 2 in more detail. As was discussed above, it turns out that the origin of these laser-induced features is *off-shell propagation* in the two-body electron-projectile system which is included in the present laser-assisted formalism via the electron-projectile eikonal phase. We can isolate in the e - P integral a term of the form

$$I_P^i \propto \left(\frac{\gamma(\mathbf{q})}{\mathbf{q} + \varepsilon} \right)^{-iZ_P/v}, \quad (38)$$

which results from the e - P interaction in the initial state. In Eq. (38), $\gamma(\mathbf{q})$ represents a collection of factors not important for the explanation of the features of interest [$\gamma(\mathbf{q}) \neq 0$ for any value of \mathbf{q}] and ε a small parameter included to avoid numerical problems. We note that the e - P integral in the CDW-EIS transition matrix also contains terms resulting from the e - P interaction in the final state, but it can be shown that those terms are well-behaved as a function of the momentum transfer \mathbf{q} as it can be extracted from the Appendix. Analyzing only the modulus of Eq. (38) we see that its magnitude diverges when $q_z(n) \approx 0$. Depending on the laser and electronic parameters, the value of $q_z(n)$ can be less or bigger than zero and consequently the term (38) will dominate the cross section when $q_z(n) \approx 0$. More explicitly we express the differential ionization cross section as

$$\frac{d\sigma^{(LA-CDW-EIS)}}{d\mathbf{k}} = \sum_n |\beta_n|^2 / |\Delta\epsilon + n\omega|^2, \quad (39)$$

where the electronic off-shell propagation of the electron-projectile part of the LA-CDW-EIS T matrix is factored out in the denominator, $1/|\Delta\epsilon + n\omega|^2$. The factor β_n is proportional to the Bessel function $J_n(\alpha)$ which largely determines the coupling to the field and the range of photon exchanges.

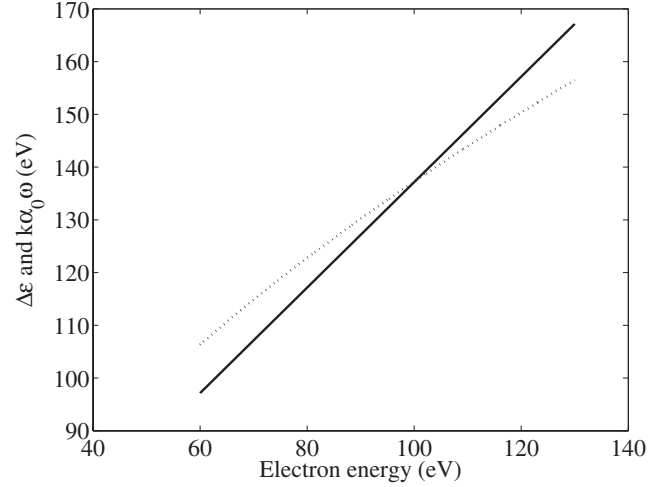


FIG. 3. Full curve: Change in electron energy $\Delta\epsilon = \epsilon_f - \epsilon_i + U_p$ as a function of electron energy, ϵ_f . Dotted curve: Approximate number of photon exchanges where the laser-electron coupling maximizes ($n \approx k\alpha_0$) times the photon energy ω as a function of electron energy, ϵ_f . Above the crossing, in the weak coupling regime, $\Delta\epsilon > k\alpha_0\omega$. Below the crossing, in the strong coupling regime, $\Delta\epsilon < k\alpha_0\omega$ (see text). The field strength is $F_0 = 0.008$ a.u., $\omega = 0.0043$ a.u.

The Bessel function is only sizable in a narrow range around the argument $\alpha = |\alpha_0 \cdot \mathbf{k}|$. The point now is that depending on $\Delta\epsilon$, this n range may give rise to (i) only positive $\Delta\epsilon + n\omega$ or (ii) positive, negative, and/or vanishing $\Delta\epsilon + n\omega$ in Eq. (39). In the latter case, the $1/|\Delta\epsilon + n\omega|^2$ factor gives rise to a sharp increase in the cross section. Figure 3 shows a crude estimate of the two regimes. Here we plot as a function of the final electron energy the electronic energy difference $\Delta\epsilon$, and the factor $k\alpha_0\omega$. Since the laser-electron coupling (and therefore β_n) peaks narrowly around $k\alpha_0$ the latter factor gives approximately the maximum of the $|n|\omega$ term of Eq. (39). Above the crossing between the two curves in Fig. 3, the photon exchanges that contribute to the cross section have $\Delta\epsilon + n\omega > 0$, and in this regime the effect of the coupling between the laser and the system is moderate as seen from Fig. 2 above the cutoff and as expected from the behavior of the energy denominator in Eq. (39). The deviation between the crossing in Fig. 3 (~ 100 eV) and the cutoff in Fig. 2 (~ 122 eV) is explained by noting that Fig. 3 is based only on the argument of the first Bessel function in Eq. (29). The second Bessel function in Eq. (29) accounts for the energy shift. We also note that above the cutoff the overall energy sharing is such that the projectile in its asymptotic motion has less energy in its final state than in its initial state ($E_f - E_i < 0$). This is the asymptotic energy condition known in the field-free case where the projectile delivers all the energy to the ionization process.

Below the cutoff in Fig. 2, the situation is significantly different. This *strong-coupling* regime corresponds crudely to the region below the crossing between the two curves in Fig. 3, and hence here there are contributions to the cross section (39) from photon exchange terms n where the denominator $\Delta\epsilon + n\omega$ changes from positive to negative and may attain values very close to zero. For a given final elec-

tron energy in this regime there exists a photon exchange number that minimizes $|\Delta\epsilon+n\omega|$ to a value close to zero and this is the reason for the general increase and emergence of a plateau below the cutoff. Particular final electron energies lead to commensurable $\Delta\epsilon$ and ω . For such a $\Delta\epsilon$, there exists a photon-exchange number such that $\Delta\epsilon+n\omega=0$ and as is clear from Eq. (39) the cross section peaks. When $\Delta\epsilon$ is commensurable with ω so is $\Delta\epsilon\pm l\omega$ with integer l . This is the reason why we predict the multiphoton peaks in Fig. 2. The off-shell propagation factor $1/|\Delta\epsilon+n\omega|$ is independent of projectile velocity and nuclear charge, and consistent herewith, we find no dependence of the position of the cutoff on these quantities. We note that in the strong-coupling plateau region, the overall sharing is such that the laser effectively pumps energy into the target-projectile system ($E_f - E_i > 0$) [13]. This happens even though no direct coupling is present. The mechanism at work is that the laser couples to the electron which again couples to the target-projectile system. The $E_f - E_i > 0$ segment is perfectly accessible, since we have overall energy conservation at asymptotic times. Before we leave the discussion of the results and Eq. (39), we stress that the present predictions depend very sensitively on the model used for the description of the field-free ion-atom scattering. By Eq. (39) the effect is traced to the off-shell propagation in the electron-projectile system which is here accounted for by an eikonal phase. Hence in FBA and DWB treatments, which are applicable in the high-energy regime characterized by the electron capture to the continuum and the binary-encounter peaks, one would expect not to find the effects reported here since these theories do not account for the initial state electron-projectile interaction coursing the present effects (see Fig. 1 and discussion above).

For the situation where the laser intensity is $F = 0.008$ a.u. we have performed time-demanding calculations using *smaller* energy steps, in order to capture the multiphoton peaks structure in detail. Taking into account that the laser frequency is $\omega = 0.117$ a.u., we expect around ten peaks in 1 eV and to be able to distinguish these peaks it would be necessary to use a step, e.g., of $\delta_e \sim 0.01$ eV. We have chosen a reasonable range of our electron spectra to perform this *high resolution* graph. To this end in Fig. 4 we can observe the electron spectra between 115 and 130 eV using an energy step of 0.01 eV. We can see clearly the peak structure and, in order to confirm our predictions concerning the energy peak distance, in the inset graph it is possible to see an even smaller fraction of the electron spectra between 121 and 124 eV. If we chose, e.g., the range between 121 and 121.5 eV we can count five peaks.

To complete our analysis, we show in Fig. 5 the electron spectrum over a larger range of energies and angles using the field-free and the LA-CDW-EIS theory. In panel (a) we show the field-free spectrum. We observe the well-known structures: (i) the electron capture to the continuum peak (ECC) when the velocity of the ionized electrons is equal to the velocity of the projectile (which in our case is $v = 10$ a.u., and for $\theta_k = 0^\circ$) [1] and (ii) the binary peak (BE) for electrons whose velocity is twice the projectile velocity v . In our 2D graph the BE peak manifests itself as a *ring* satisfying $k_{BE} = 2v \cos \theta_k$. Using a LA-CDW-EIS theory for the collision part, we assure the correct description of all the structures

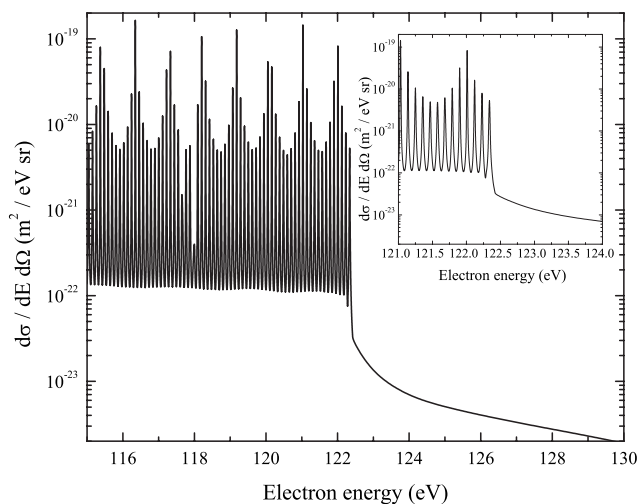


FIG. 4. Electron emission spectrum in the laser-assisted ion-atom collision $p^+ + H(1s) \rightarrow p^+ + p^+ + e^-$ for the geometry and velocity as in Fig. 1 and $F = 0.008$ a.u. using LA-CDW-EIS theory. We have used a *resolution* in the electron energy of 0.01 eV to capture in detail the multiphoton peak structure. The inset graph shows the region between 121 and 124 eV.

described above. Panel (b) shows the result when the laser field is present (the white triangles with no data are due to the restriction of the present theory to the $\mathbf{A}_0 \cdot \mathbf{r}_T / \alpha_0 \cdot \mathbf{k} \ll 1$ segment (see Sec. II for details). We observe an enhancement in the cross section below the ECC peak and a *splitting* of the BE peak that can be explained using classical considerations and which also appear in first order theories (see e.g., [4,5,10]). The enhancement of the low-energy cross section is also seen in directions with nonvanishing k_\perp . In these cases, however, the effect is less pronounced simply due to the reduction of the coupling parameter $\alpha_0 \cdot \mathbf{k}$.

IV. CONCLUSION

In conclusion, we have reported theoretical predictions of high-energy ionizing laser-assisted ion-atom collisions. The predicted effects (i) plateau, (ii) cutoff, and (iii) multiphoton peak structures are all identified as being due to dynamics in the initial target electron-projectile interaction as presented by the eikonal phase in the present formalism. Accordingly, the effects are present in the results obtained with the LA-CDW-EIS theory but absent in the LA-DWB and LA-FBA theories. The criteria for the emergence of these features is that the parameter characterizing the laser-electron coupling in the continuum, $k\alpha_0\omega$ expressed in terms of the momentum k , quiver radius α_0 , and frequency, ω , is of the order or larger than the change in the electronic energy, $\Delta\epsilon$. Experimental investigations of the predicted effects are entirely possible with current laser beam and detection technologies. The use of a CO₂ laser not only makes high-order free-free transitions more likely, it also makes our study experimentally feasible. The CO₂ laser has a long pulse and for all practical purposes it may be assumed to be monochromatic and present during the scattering events. Hence the assisting field used in the present simulations introduce no synchronization

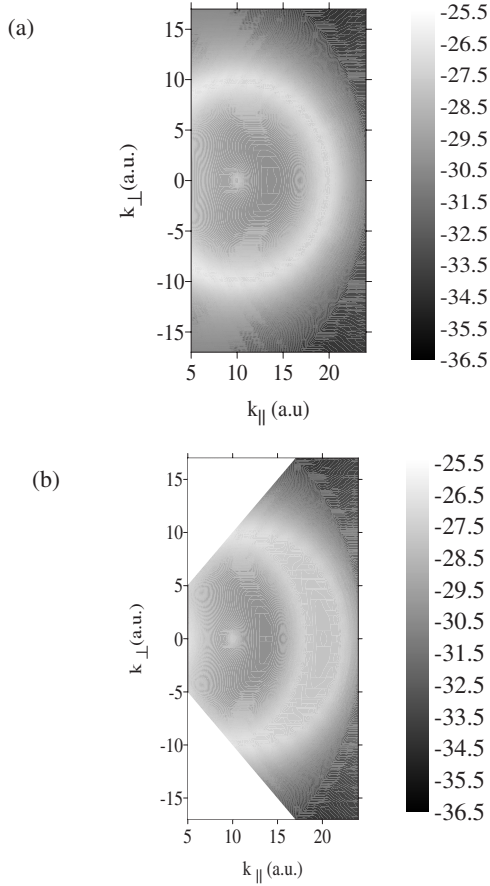


FIG. 5. Electron emission spectrum in the laser-assisted ion-atom collision $p^+ + \text{H}(1s) \rightarrow p^+ + p^+ + e^-$. The shading scale corresponds to the logarithm of the cross section (29). The projectile parameters are as in Fig. 1. The electron emission angle is $\theta_k = \tan^{-1}(k_{\perp}/k_{\parallel})$, where \parallel (\perp) indicates the direction of the outgoing electron with respect to the incoming projectile. (a) Field-free spectrum and (b) laser-assisted spectrum using the LA-CDW-EIS formalism for $F_0 = 0.008$ a.u. (2.25×10^{12} W/cm²). Only the spectrum where $\mathbf{A}_0 \cdot \mathbf{r}_T / \alpha_0 \cdot \mathbf{k} \ll 1$ is shown; hence the white triangles.

or counting rate problems. As an alternative to heavy-ion projectiles one could use fast electrons ($v \sim 10$ a.u.) and study the laser-induced phenomena in (e - $2e$) experiments [25].

ACKNOWLEDGMENTS

We thank J. F. McCann and J. M. Rost for useful comments. This work was supported by the Danish Agency of Science, Technology and Innovation (Grant No. 2117-05-0081).

APPENDIX

In this appendix we give the explicit expressions for the integrals that conform the field-free CDW-EIS T matrix in the prior version. For the *scalar* integrals $I_P(\mathbf{q})$ and $I_T(\mathbf{q})$ it is possible to write

$$I_P(\mathbf{q}) = \frac{(2\pi)^{-3}}{2} N(\alpha_P)^* \int d\mathbf{r}_P \exp(-i\mathbf{q} \cdot \mathbf{r}_P - \varepsilon r_P) \quad (\text{A1})$$

$$\times \left\{ \nabla_{\mathbf{r}_P}^2 \exp \left[-i \frac{Z_P}{v} \ln(vr_P + \mathbf{v} \cdot \mathbf{r}_P) \right] \right\} \\ \times {}_1F_1(i\alpha_P, 1, ik_P r_P + i\mathbf{k}_P \cdot \mathbf{r}_P) \quad (\text{A2})$$

and

$$I_T(\mathbf{q}) = (2\pi)^{-3} N(\alpha_T)^* \int d\mathbf{r}_T \exp[i(\mathbf{q} - \mathbf{k}) \cdot \mathbf{r}_T] \quad (\text{A3})$$

$$\times \phi_i(r_T) {}_1F_1(i\alpha_T, 1, ikr_T + i\mathbf{k} \cdot \mathbf{r}_T), \quad (\text{A4})$$

respectively. We have added a positive integrating factor ε . The integral $I_P(\mathbf{q})$ containing the Laplacian of the eikonal phase can be reduced as is done in, e.g., [26]. Consequently we have to solve for $I_P(\mathbf{q})$ an integral of the form

$$I_P(\mathbf{q}) = \frac{(2\pi)^{-3}}{2} N(\alpha_P)^* \frac{Z_P^2}{v} \int d\mathbf{r}_P \exp(-i\mathbf{q} \cdot \mathbf{r}_P - \varepsilon r_P) \quad (\text{A5})$$

$$\times \frac{\exp \left[-i \left(\frac{Z_P}{v} - i \right) \ln(vr_P + \mathbf{v} \cdot \mathbf{r}_P) \right]}{r_P} \\ \times {}_1F_1(i\alpha_P, 1, ik_P r_P + i\mathbf{k}_P \cdot \mathbf{r}_P). \quad (\text{A6})$$

Analytical expressions for $I_P(\mathbf{q})$ and $I_T(\mathbf{q})$ can be obtained:

$$I_P(\mathbf{q}) = \frac{(2\pi)^{-3}}{2} N(\alpha_P)^* \frac{Z_P^2 4\pi}{v D_P} \gamma(\alpha_i) A_1^{-i\alpha_P} U_2^{-i\alpha_i} F(x_2) \quad (\text{A7})$$

with $\alpha_i = \frac{Z_P}{v} - i$ and where

$$D_P = q^2 + \varepsilon^2, \quad (\text{A8})$$

$$S_1 = -\mathbf{k}_P \cdot \mathbf{q} - i\varepsilon k_P, \quad (\text{A9})$$

$$S_2 = -\mathbf{v} \cdot \mathbf{q} - i\varepsilon v, \quad (\text{A10})$$

$$S_3 = k_P v - \mathbf{k}_P \cdot \mathbf{v}, \quad (\text{A11})$$

$$U_j = 2S_j / D_P, \quad A_j = 1 + U_j, \quad j = 1, 2, 3, \quad (\text{A12})$$

$$F(x) = {}_2F_1(i\alpha_P, i\alpha_i, 1, x), \quad (\text{A13})$$

$$x_2 = 1 - \frac{(U_2 - U_3)}{A_1 U_2}, \quad (\text{A14})$$

$$\gamma(a) = \exp\left(\frac{1}{2}\pi a\right) \Gamma(1 - ia), \quad (\text{A15})$$

and

$$I_T(\mathbf{q}) = \frac{(2\pi)^{-3}}{2} N(\alpha_P)^* N_i \frac{4\pi}{D_T^2} A_T^{-i\alpha_T} \left(2Z_T - i\alpha_T \frac{B_T}{A_T} \right), \quad (\text{A16})$$

where

$$D_T = |q - k|^2 + Z_T^2, \quad (\text{A17})$$

$$S_T = \mathbf{k} \cdot (\mathbf{q} - \mathbf{k}) - iZ_T k, \quad (\text{A18})$$

$$U_T = 2S_T/D_T, \quad A_T = 1 + U_T, \quad (\text{A19})$$

$$B_T = 2(ik + Z_T U_T). \quad (\text{A20})$$

In $I_T(\mathbf{q})$ we have considered a hydrogenic $1s$ state $\phi_i(r_T) = N_i e^{-Z_T r_T}$.

On the other hand, the *vectorial* integrals of the CDW-EIS T matrix can be written

$$\mathbf{J}_P(\mathbf{q}) = \frac{(2\pi)^{-3}}{2} N(\alpha_P)^* \int d\mathbf{r}_P \exp(-i\mathbf{q} \cdot \mathbf{r}_P - \varepsilon r_P) \quad (\text{A21})$$

$$\times \left\{ \nabla_{\mathbf{r}_P} \exp \left[-i \frac{Z_P}{v} \ln(vr_P + \mathbf{v} \cdot \mathbf{r}_P) \right] \right\} \times {}_1F_1(i\alpha_P, 1, ik_P r_P + i\mathbf{k}_P \cdot \mathbf{r}_P) \quad (\text{A22})$$

and

$$\mathbf{J}_T(\mathbf{q}) = (2\pi)^{-3} N(\alpha_T)^* \int d\mathbf{r}_T \exp[i(\mathbf{q} - \mathbf{k}) \cdot \mathbf{r}_T] \quad (\text{A23})$$

$$\times [\nabla_{\mathbf{r}_T} \phi_i(r_T)] {}_1F_1(i\alpha_T, 1, ikr_T + i\mathbf{k} \cdot \mathbf{r}_T), \quad (\text{A24})$$

respectively. Using the definitions (A8)–(A14) we can write $\mathbf{J}_P(\mathbf{q})$ as

$$\mathbf{J}_P(\mathbf{q}) = (2\pi)^{-3} N(\alpha_P)^* \frac{8\pi i Z_P}{D_P^2 v} \gamma \left(\frac{Z_P}{v} \right) A_1^{-i\alpha_P} U_2^{-iZ_P/v-1} \times [J_{91} \mathbf{k}_P + J_{92} \mathbf{v} - J_{93} \mathbf{q}] \quad (\text{A25})$$

with

$$J_{91} = -i \frac{\alpha_P v}{A_1} F^+(x_2), \quad (\text{A26})$$

$$J_{92} = i\varepsilon F(x_2) + i \frac{\alpha_P}{A_1} F^+(x_2) \left(k_P + i\varepsilon \frac{U_3}{U_2} \right), \quad (\text{A27})$$

$$J_{93} = -i \frac{\alpha_P v U_3}{U_2 A_1} F^+(x_2) - v F(x_2), \quad (\text{A28})$$

and now

$$F(x) = {}_2F_1 \left(i\alpha_P, i \frac{Z_P}{v}, 1, x \right), \quad (\text{A29})$$

$$F^+(x) = {}_2F_1 \left(i\alpha_P + 1, i \frac{Z_P}{v} + 1, 2, x \right). \quad (\text{A30})$$

Finally using Eqs. (A17)–(A20) $\mathbf{J}_T(\mathbf{q})$ is

$$\mathbf{J}_T(\mathbf{q}) = - (2\pi)^{-3} N(\alpha_T)^* Z_T N_i \frac{8\pi i}{D_T^2} A_T^{-i\alpha_T} \times \left[\frac{i\alpha_T}{A_T} \mathbf{k} + \left(1 - i\alpha_T + \frac{i\alpha_T}{A_T} \right) (\mathbf{q} - \mathbf{k}) \right], \quad (\text{A31})$$

where we have exploited that $\nabla_{\mathbf{r}_T} \phi_i(r_T) = -N_i Z_T \hat{\mathbf{r}}_T e^{-Z_T r_T}$.

-
- [1] N. Stolterfoht, R. D. Dubois, and R. D. Rivarola, *Electron Emission in Heavy Ion-Atom Collisions* (Springer, Berlin, 1997).
- [2] P. B. Corkum, Phys. Rev. Lett. **71**, 1994 (1993).
- [3] M. Lein and J. M. Rost, Phys. Rev. Lett. **91**, 243901 (2003).
- [4] A. B. Voitkiv and J. Ullrich, J. Phys. B **34**, 1673 (2001).
- [5] A. B. Voitkiv and J. Ullrich, J. Phys. B **34**, 4383 (2001).
- [6] T. Kirchner, Phys. Rev. Lett. **89**, 093203 (2002).
- [7] L. B. Madsen, J. P. Hansen, and L. Kocbach, Phys. Rev. Lett. **89**, 093202 (2002).
- [8] S. M. Li, J. Chen, and Z. F. Zhou, J. Phys. B **35**, 557 (2002).
- [9] T. Kirchner, Phys. Rev. A **69**, 063412 (2004).
- [10] M. F. Ciappina and L. B. Madsen, J. Phys. B **39**, 5037 (2006).
- [11] F. Anis, V. Roudnev, R. Cabrera-Trujillo, and B. D. Esry, Phys. Rev. A **73**, 043414 (2006).
- [12] T. Kirchner, Phys. Rev. A **75**, 025401 (2007).
- [13] L. Feng and Y.-k. Ho, Eur. Phys. J. D **7**, 25 (1999); L. Feng and Y.-k. Ho, Phys. Lett. A **264**, 131 (1999); L. Feng and Y.-k. Ho, Phys. Rev. A **61**, 023407 (2000).
- [14] D. S. F. Crothers and J. F. McCann, J. Phys. B **16**, 3229 (1983).
- [15] P. D. Fainstein, V. H. Ponce, and R. D. Rivarola, J. Phys. B **24**, 3091 (1991).
- [16] D. S. F. Crothers and L. J. Dubé, Adv. At., Mol., Opt. Phys. **16**, 3229 (1983).
- [17] M. Abramowitz and I. Stegun, *Handbook of Mathematical Functions* (Dover, New York, 1964).
- [18] M. Jain and N. Tzoar, Phys. Rev. A **18**, 538 (1978).
- [19] P. Cavaliere, G. Ferrante, and C. Leone, J. Phys. B **13**, 4495 (1980).
- [20] G. L. Yudin, S. Patchkovskii, P. B. Corkum, and A. D. Bandrauk, J. Phys. B **40**, F93 (2007).
- [21] I. S. Gradshteyn and I. M. Ryzhik, *Table of Integrals, Series and Products*, 6th ed. (Academic Press, San Diego, 2000).
- [22] C. Joachain, *Quantum Collision Theory* (North-Holland, Amsterdam, 1975).
- [23] A. Weingartner, J. K. Holmes, J. Sabagh, and S. L. Chin, J. Phys. B **16**, 1805 (1983).
- [24] N. M. Kroll and K. M. Watson, Phys. Rev. A **8**, 804 (1973).
- [25] C. Höhr, A. Dorn, B. Najjari, D. Fischer, C. D. Schröter, and J. Ullrich, Phys. Rev. Lett. **94**, 153201 (2005).
- [26] M. S. Gravielle and J. E. Miraglia, Comput. Phys. Commun. **69**, 53 (1992).